
This is an electronic reprint of the original article.
This reprint may differ from the original in pagination and typographic detail.

Pirsto, Ville; Kukkola, Jarno; Rahman, F M Mahafugur; Hinkkanen, Marko
Real-time identification method for LCL filters used with grid converters

Published in:
Proceedings of the 11th IEEE Energy Conversion Congress and Exposition, ECCE 2019

DOI:
[10.1109/ECCE.2019.8912289](https://doi.org/10.1109/ECCE.2019.8912289)

Published: 29/09/2019

Document Version
Peer-reviewed accepted author manuscript, also known as Final accepted manuscript or Post-print

Please cite the original version:
Pirsto, V., Kukkola, J., Rahman, F. M. M., & Hinkkanen, M. (2019). Real-time identification method for LCL filters used with grid converters. In *Proceedings of the 11th IEEE Energy Conversion Congress and Exposition, ECCE 2019* (pp. 3729-3736). (IEEE Energy Conversion Congress and Exposition). IEEE.
<https://doi.org/10.1109/ECCE.2019.8912289>

This material is protected by copyright and other intellectual property rights, and duplication or sale of all or part of any of the repository collections is not permitted, except that material may be duplicated by you for your research use or educational purposes in electronic or print form. You must obtain permission for any other use. Electronic or print copies may not be offered, whether for sale or otherwise to anyone who is not an authorised user.

© 2019 IEEE. This is the author's version of an article that has been published by IEEE. Personal use of this material is permitted. Permission from IEEE must be obtained for all other uses, in any current or future media, including reprinting/republishing this material for advertising or promotional purposes, creating new collective works, for resale or redistribution to servers or lists, or reuse of any copyrighted component of this work in other works.

Real-time Identification Method for LCL Filters Used With Grid Converters

Ville Pirsto, Jarno Kukkola, F. M. Mahafugur Rahman, and Marko Hinkkanen
Aalto University School of Electrical Engineering
Espoo, Finland

Abstract—This paper presents a real-time algorithm for identifying the inductance and capacitance values of LCL filters used with grid converters. As a side product, the grid inductance seen from the point of common coupling is also estimated. A wideband excitation signal is added to the converter voltage reference. During the excitation, the converter currents and the converter voltage reference are sampled. The samples are preprocessed in real time by removing DC biases and significant grid-frequency harmonics. Parameters of a discrete-time model are estimated at each sampling instant with a recursive estimation algorithm. The model parameter estimates are translated into inductance and capacitance values. The method can be embedded to a control system of PWM-based converters in a plug-in manner. Only the DC-link voltage and converter currents need to be measured. Simulation and experimental results are presented for a 12.5-kVA grid converter system to evaluate the proposed method.

Index Terms—Grid converter, LCL filter, real-time identification, recursive parameter estimation

I. INTRODUCTION

In the last decade, the cost of producing electricity using renewable energy resources, such as wind and solar, has reduced greatly. As a result, the penetration of renewable energy sources in the electric grid has increased enormously. These renewable energy sources are connected to the grid through a converter equipped with a filter, typically of an L or LCL type. The LCL filter has gained popularity due to its higher attenuation above its resonance frequency compared to an L filter of equal magnetic volume [1]. However, the resonant modes of the LCL filter make the control of the converter more challenging. These resonant modes are typically damped with active damping methods that are implemented in the converter control systems. Many of the active damping methods require knowledge of the filter parameters, e.g., [2]–[5].

Even if the nominal parameters of the LCL filter are known, manufacturing tolerances and aging phenomena cause uncertainties in the parameters. If the physical parameters of the LCL filter could be identified on converter startup and readily during operation, adaptive control could be employed for improved performance [6]. Additionally, knowledge of the changes in the filter parameters could potentially be used for condition monitoring and fault diagnosis, e.g., tracking long-term evolution of the filter capacitances for pre-emptive maintenance [7].

Closely related to the identification of an LCL filter, there are numerous methods proposed for real-time identification

of the grid impedance, e.g., [8]–[13]. The identification has been carried out using Fourier analysis [8], recursive parameter estimation [9], [10], model predictive control [11], extended Kalman filter [12], and wavelets [13].

Off-line methods for identifying the LCL filter of a grid converter have been proposed in [14]–[17]. In [14]–[16], methods for identifying a discrete-time state-space model of the LCL filter are presented. In [17], the inductance and capacitance values of the LCL filter are identified offline using an indirect identification approach. In [18], the values of these LCL filter parameters are identified as an online batch process, yielding estimates during operation each time the identification method is run. Despite the number of different methods proposed for real-time identification of the grid impedance, no real-time identification method for parameters of an LCL filter has yet been proposed.

In this paper, an enhanced version of method [18] is proposed with the following improvements:

- 1) The proposed method can run continuously to provide real-time estimates of the filter parameters and the grid inductance.
- 2) The number of parameter estimation algorithms is reduced to one, simplifying the identification method without compromising accuracy.

Additionally, the proposed real-time implementation allows for distributing the computational costs over the run time of the algorithm. Simulation and experimental results are presented for a 12.5-kVA grid converter.

II. SYSTEM MODEL

A space-vector model for an ideal LCL filter connected between the converter and the grid is shown in Fig. 1, where L_{fc} is the converter-side inductance, C_f the filter capacitance, L_{fg} the grid-side inductance, and L_g the grid inductance. In the identification method, the grid inductance L_g is included in the estimate of the grid-side inductance, i.e., the method estimates the sum $L_{gt} = L_{fg} + L_g$. A lossless model is assumed in order to simplify the proposed method. A hold-equivalent discrete-time model of the LCL filter in stationary coordinates can be written as

$$\begin{aligned} \mathbf{x}(k+1) &= \Phi \mathbf{x}(k) + \Gamma_c \mathbf{u}_c(k) + \Gamma_g \mathbf{u}_g(k) \\ \mathbf{i}_c(k) &= \mathbf{C}_c \mathbf{x}(k) \end{aligned} \quad (1)$$

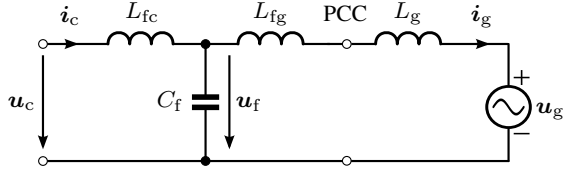


Fig. 1. Circuit model of an ideal LCL filter connected to an inductive grid in stationary coordinates.

where $\mathbf{x} = [i_c, \mathbf{u}_f, i_g]^T$ is the state vector and $\mathbf{C}_c = [1, 0, 0]$. The system matrices Φ , Γ_c , and Γ_g can be calculated from their continuous-time counterparts (cf. Appendix A).

Due to the finite computation time of the control algorithm, the converter voltage reference $\mathbf{u}_{c,\text{ref}}$ is delayed by one sampling period, i.e., $\mathbf{u}_c(k) = z^{-1}\mathbf{u}_{c,\text{ref}}(k)$, where z^{-1} is the backward-shift operator. Taking the computational delay into account, the converter current i_c can be obtained from the state-space model (1) as

$$i_c(k) = Y_c(z)\mathbf{u}_{c,\text{ref}}(k) + Y_g(z)\mathbf{u}_g(k) \quad (2)$$

where the pulse transfer operator $Y_c(z)$ is given by

$$Y_c(z) = z^{-1}\mathbf{C}_c(z\mathbf{I} - \Phi)^{-1}\Gamma_c \quad (3)$$

and the pulse transfer operator $Y_g(z)$ is obtained similarly. A block diagram representation of the discrete-time LCL filter model (2) is shown in Fig. 2. Knowledge of the structure of $Y_c(z)$ is important for selecting a suitable identification model, and it can be expressed as

$$Y_c(z) = \frac{B(z)}{A(z)} = \frac{z^{-1}(b_1z^{-1} + b_2z^{-2} + b_1z^{-3})}{1 + a_1z^{-1} - a_1z^{-2} - z^{-3}} \quad (4)$$

where [17]

$$\begin{aligned} a_1 &= -1 - 2\cos(\omega_p T_s) \\ b_1 &= \frac{T_s + L_{gt} \sin(\omega_p T_s)/(\omega_p L_{fc})}{L_{fc} + L_{gt}} \\ b_2 &= -\frac{2T_s \cos(\omega_p T_s) + 2L_{gt} \sin(\omega_p T_s)/(\omega_p L_{fc})}{L_{fc} + L_{gt}} \end{aligned} \quad (5)$$

where T_s is the sampling period of the converter control system and ω_p is the resonance frequency of the LCL filter given by

$$\omega_p = \sqrt{\frac{L_{fc} + L_{gt}}{L_{fc} C_f L_{gt}}} \quad (6)$$

III. IDENTIFICATION MODEL

Choice of the identification model structure is crucial for obtaining accurate results. The most common discrete-time identification model structures are divided into equation-error and output-error models [19]. Equation-error models include an error term that passes through the same denominator polynomial as the input signal. Such models correspond well to the model of an LCL filter, as both inputs $\mathbf{u}_{c,\text{ref}}$ and \mathbf{u}_g pass through the same denominator polynomial $A(z)$ to i_c . Therefore, an autoregressive-moving-average (ARMAX)

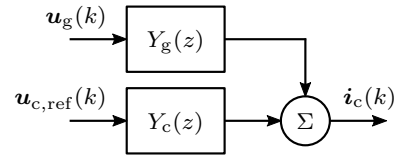


Fig. 2. Block diagram representation of the discrete-time LCL filter model.

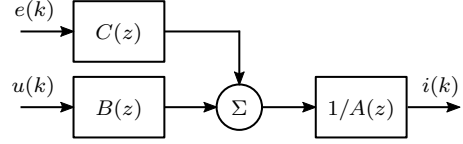


Fig. 3. ARMAX model structure.

equation-error model, shown in Fig. 3, is used. Out of the available equation-error models, ARMAX is selected due to the flexibility it offers for modelling the error term. The discrete-time ARMAX model can be expressed as [19]

$$A(z)i(k) = B(z)u(k) + C(z)e(k) \quad (7)$$

where $i(k)$ is the preprocessed converter current $i_c(k)$ corresponding to the model output, $u(k)$ is the preprocessed converter voltage reference $\mathbf{u}_{c,\text{ref}}(k)$ corresponding to the model input, and $e(k)$ represents white noise with zero mean. The structures of polynomials $A(z)$ and $B(z)$ are selected identical to the denominator and the numerator of $Y_c(z)$ given in (4), respectively. As a result, the parameters in polynomials $A(z)$ and $B(z)$ of the identification model (7) can be related to the parameters of the LCL filter through (5). For describing the noise, a second-order polynomial

$$C(z) = 1 + c_1z^{-1} + c_2z^{-2} \quad (8)$$

is found sufficient.

If the identification model (7) is compared to the equation (2) for the converter current, it can be observed that it does not include the effect of the grid voltage \mathbf{u}_g . However, this exclusion does not pose a problem since the significant components of the grid voltage \mathbf{u}_g are removed by preprocessing the input-output data, as will be discussed in Section IV-B. Minor components originating from the grid voltage are mostly modeled by the noise term.

The ARMAX model (7) can be written as a regression model

$$y(k) = \varphi^T(k)\theta + e(k) \quad (9)$$

where the regressed variable is

$$y(k) = i(k) - i(k-3) \quad (10)$$

and the regressor vector φ and the parameter vector θ are

$$\varphi(k) = \begin{bmatrix} i(k-2) - i(k-1) \\ u(k-2) + u(k-4) \\ u(k-3) \\ e(k-1) \\ e(k-2) \end{bmatrix} \quad \theta = \begin{bmatrix} a_1 \\ b_1 \\ b_2 \\ c_1 \\ c_2 \end{bmatrix} \quad (11)$$

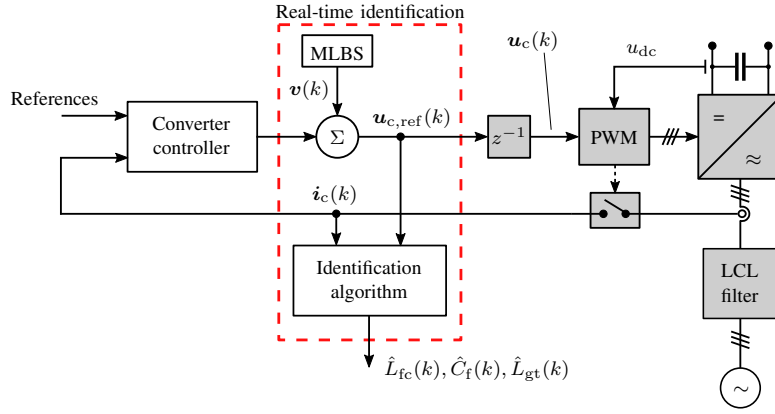


Fig. 4. Block diagram of the identification method embedded to a grid converter system.

respectively. The parameter vector includes the model parameters of polynomials (4) and (8). The regression model (9) will be employed in the identification method as described in the next section.

IV. IDENTIFICATION METHOD

A block diagram of the proposed identification method embedded to a PWM-based grid converter system is presented in Fig. 4. Sampling of the converter currents is synchronized with the PWM and the digital control system is assumed to cause a delay of one sampling period. The DC bus voltage u_{dc} is measured for the PWM and the converter current i_c is controlled by the converter.

A block diagram of the identification algorithm is presented in Fig. 5. While the system is being excited by a wideband excitation signal $v(k)$, the following steps are taken at each sampling period:

- A) Converter voltage reference $u_{c,ref}$ and converter currents i_c are sampled.
- B) Samples of the converter voltage reference and converter currents are preprocessed by removing the significant grid-frequency harmonics from the acquired samples.
- C) Estimates of the ARMAX model parameters $\hat{\theta}$ are updated.
- D) Parameter estimates $\hat{\theta}$ are translated into inductance and capacitance estimates \hat{L}_{fc} , \hat{C}_f , and \hat{L}_{gt} .

A. Excitation and Sampling

During identification, an excitation signal $v(k) = v_\alpha(k) + jv_\beta(k)$ is added to the converter voltage reference calculated by the converter control system, as shown in Fig. 4. In order to successfully identify the LCL filter, the power spectrum of the excitation signal should be wide enough to excite the resonance frequency (6) of the LCL filter sufficiently. A maximum-length binary sequence (MLBS) is used as the excitation signal due to its ease of implementation, deterministic behavior, repeatability, wide power spectrum, and lowest possible crest factor [19], [20]. In this paper, the MLBS is injected into v_β while $v_\alpha = 0$. As a result, only the b and c phases are excited and thus only the imaginary components of

the sampled signals are processed. This slightly increases the accuracy of the parameter estimation as the effect of inverter nonlinearities is reduced [18]. The choice of amplitude of the MLBS signal is a compromise between excitation power and distortion of the grid currents.

B. Harmonic Removal

In practice, the grid voltage includes some low-order harmonics in addition to its fundamental component. In order to increase the accuracy of the parameter estimates obtained from the method, significant grid-frequency harmonics should be removed from the current and voltage samples to eliminate the effect of the grid voltage on the estimates. The selected harmonic components are removed from the samples as

$$u(k) = u_{c\beta,ref}(k) - \sum_m u_m(k) \quad (12)$$

$$i(k) = i_{c\beta}(k) - \sum_m i_m(k) \quad (13)$$

where u_m and i_m are the m th-order harmonics for the voltage and current, respectively. In this paper, the harmonic components $m = [0, 1, 5, 7]$ are removed from the samples. As a result, the sum in (12) becomes $\sum_m u_m(k) = u_0(k) + u_1(k) + u_5(k) + u_7(k)$ and the sum in (13) can be written similarly. The DC component $m = 0$ is removed due to a possible bias in the measurement sensors.

There are several different algorithms for computing harmonic components from a signal, the standard method for batch processes being the discrete Fourier transform (DFT). The DFT of a signal, e.g., current i , calculated from N previous samples at time k for a m th-order harmonic can be expressed as

$$I_m(k) = \sum_{n=0}^{N-1} i(q+n) \mathbf{W}_N^{-mn} \quad \forall m \in \{0 \dots N-1\} \quad (14)$$

where $q = k - N + 1$ and $\mathbf{W}_N = e^{j2\pi/N}$ [21].

For computing a limited number of harmonics efficiently in real time on a sample-by-sample basis, sliding DFT (SDFT) algorithms are a superior tool. The SDFT algorithms leverage the fact that only one element in the sample buffer changes

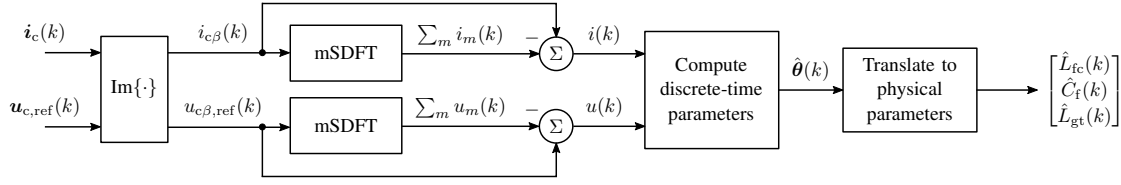


Fig. 5. Block diagram of the proposed identification method.

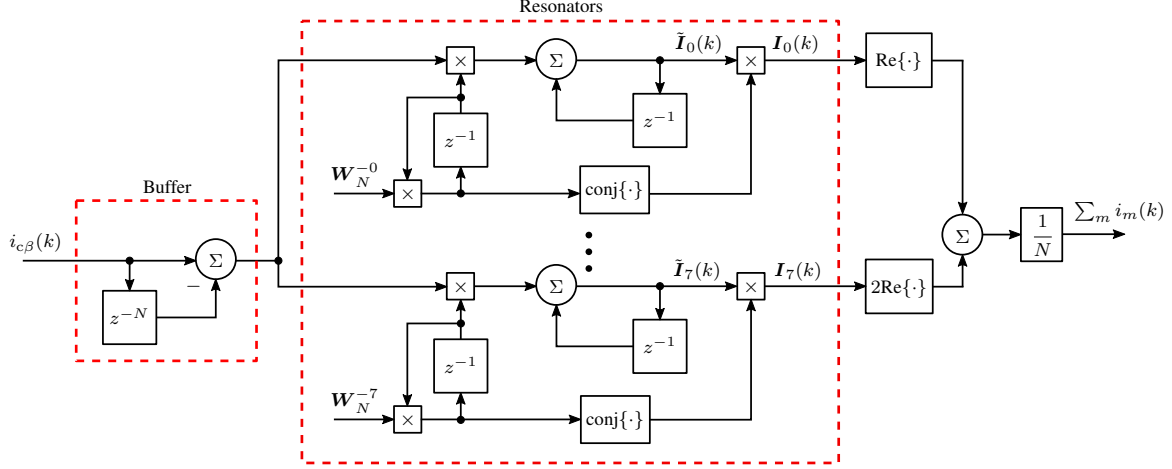


Fig. 6. Block diagram representation of the mSDFT algorithm for $m = [0, 1, 5, 7]$. The output consists of four frequency components $\sum_m i_m(k) = i_0(k) + i_1(k) + i_5(k) + i_7(k)$.

between the sampling instants by modifying the result of the DFT from the previous sampling instant accordingly. The traditional SDFT can be derived from (14) as [22]

$$\mathbf{I}_m(k) = \mathbf{W}_N^{-mn} [\mathbf{I}_m(k-1) + i(k) - i(k-N)] \quad (15)$$

where $n = \text{mod}(k, N)$. However, this form of the SDFT suffers from numerical instabilities and accumulated errors due to a complex pole on the unit circle [23]. Hence, a guaranteed stable and accurate variant of the sliding DFT, the modulated sliding DFT (mSDFT), is used instead [23]. The structure of the mSDFT is presented in Fig. 6, which depicts the extraction of the harmonics from the converter current samples used in the identification. The mSDFT consists of a comb filter acting as a sample buffer and one resonator for tracking each harmonic of interest. Mathematically, N -point mSDFT of a signal, e.g., current i , at time k for a m th-order harmonic can be expressed as [23]

$$\tilde{\mathbf{I}}_m(k) = \tilde{\mathbf{I}}_m(k-1) + \mathbf{W}_N^{-mn} [i(k) - i(k-N)] \quad (16)$$

$$\mathbf{I}_m(k) = \mathbf{W}_N^{m(n+1)} \tilde{\mathbf{I}}_m(k) \quad (17)$$

where the tilde indicates that the DFT bin calculated in (16) has phase error that is corrected with (17). Finally, as shown in Fig. 6, the spectral bins are transformed into instantaneous values of the harmonics as

$$i_m(k) = \begin{cases} \frac{1}{N} \text{Re}\{\mathbf{I}_m(k)\} & \text{if } m = 0 \\ \frac{2}{N} \text{Re}\{\mathbf{I}_m(k)\} & \text{else} \end{cases} \quad (18)$$

C. Model Parameter Estimation

A recursive prediction error (RPE) algorithm [24] is used for computing the estimates \hat{a}_1 , \hat{b}_1 , and \hat{b}_2 of the ARMAX model parameters a_1 , b_1 , and b_2 (cf. Appendix B). Estimates for the noise polynomial parameters \hat{c}_1 and \hat{c}_2 are also obtained in the process.

For tracking time-varying parameters with the RPE algorithm, either a forgetting factor λ less than unity needs to be used or the covariance matrix \mathbf{P} needs to be actively modified. If neither of these modifications is employed, the tracking capability of time-varying parameters is severely hindered due to the covariance wind-up phenomenon [6]. In the covariance wind-up, the values of a number of elements in the covariance matrix tend to zero, causing the estimation algorithm to become insensitive to certain parameter changes.

1) *Constant Forgetting Factor*: If a forgetting factor less than unity is used, i.e., $\lambda < 1$, the elements of the covariance matrix \mathbf{P} are prevented from tending to zero. The smaller the forgetting factor is, the more sensitive the estimation algorithm becomes to parameters changes. However, decreasing the forgetting factor causes the estimation algorithm to become more sensitive to noise and thus realistic values for the forgetting factor are often limited close to unity [24].

2) *Variable Forgetting Factor*: Another possible modification is to modify the covariance matrix \mathbf{P} actively during operation based on some predetermined condition for which there are numerous different possibilities [6], [25]. For example, the diagonal elements can be modified based on the trace of

the matrix or the whole covariance matrix can be modified regularly based on time k .

As the RPE algorithm is a gradient method, the algorithm might temporarily stray from the correct parameter estimate vector if the covariance matrix is modified too aggressively. Therefore, the covariance matrix is indirectly modified by altering the forgetting factor during the operation. This alteration amounts to scaling each element of the covariance matrix proportionally to its value to avoid aggressive modifications (cf. Appendix B). As a result, consistent parameter estimates are obtained. In this case, the forgetting factor can be expressed as a function of time k as

$$\lambda(k) = \begin{cases} x & \text{if } \text{mod}(k, M) = 0 \\ 1 & \text{else} \end{cases} \quad (19)$$

where $x < 1$ and M is the number of samples between modifications of the covariance matrix. The selection of M should be based on how frequently the parameter estimates are required and on the available computational resources.

One of the benefits of regular modification of the covariance matrix compared to using a constant forgetting factor less than unity is that the estimates converge quickly to a less noisy value after modification of the covariance matrix due to the unity forgetting factor. Therefore, the most accurate parameter estimates between covariance matrix modifications can be obtained right before the forgetting factor is altered. Instead of updating the inductance and capacitance estimates each sampling period, the estimates can be updated only once every M samples in this case. Mathematically, the parameter estimates are updated at time k if $\text{mod}(k, M) = M - 1$. Furthermore, as the estimates are updated more seldom, computational resources can be saved. A drawback of this modification is that the parameter variations are not immediately seen in the estimates.

D. Translation to Inductance and Capacitance Values

Finally, the discrete-time model parameter estimates are translated into inductance and capacitance values by expressing the parameters L_{fc} , C_f , and L_{gt} as functions of the discrete-time model parameters a_1 , b_1 , and b_2 in (4) as [17]

$$\begin{aligned} \hat{\omega}_p &= \frac{1}{T_s} \cos^{-1} \left(-\frac{\hat{a}_1 + 1}{2} \right) \\ \hat{L}_{fc} &= \frac{2 \frac{\sin(\hat{\omega}_p T_s)}{\hat{\omega}_p} [\cos(\hat{\omega}_p T_s) - 1]}{2\hat{b}_1 \left[\cos(\hat{\omega}_p T_s) - \frac{\sin(\hat{\omega}_p T_s)}{\hat{\omega}_p T_s} \right] + \hat{b}_2 \left[1 - \frac{\sin(\hat{\omega}_p T_s)}{\hat{\omega}_p T_s} \right]} \\ \hat{L}_{gt} &= -\frac{\hat{\omega}_p \hat{L}_{fc} [\hat{L}_{fc} \hat{b}_2 + 2T_s \cos(\hat{\omega}_p T_s)]}{\hat{\omega}_p \hat{L}_{fc} \hat{b}_2 + 2 \sin(\hat{\omega}_p T_s)} \\ \hat{C}_f &= \frac{\hat{L}_{fc} + \hat{L}_{gt}}{\hat{\omega}_p^2 \hat{L}_{fc} \hat{L}_{gt}} \end{aligned} \quad (20)$$

where the dependency on time k is omitted to maintain a level of simplicity. The above equations are calculated every sampling period for a constant forgetting factor and once every M sampling periods for a variable forgetting factor.

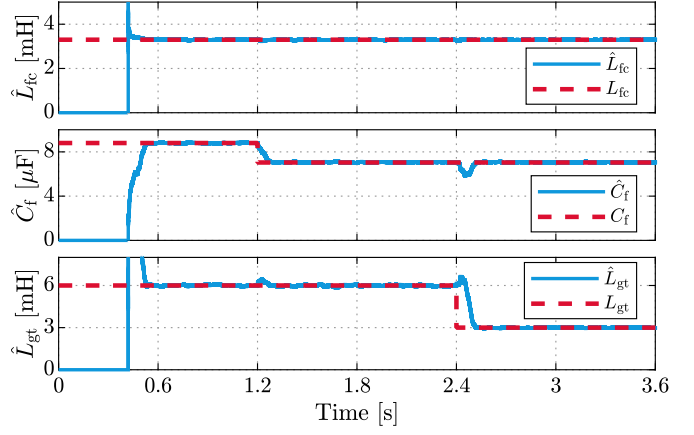


Fig. 7. Simulated evolution of the LCL filter parameter estimates with $\lambda = 0.995$ assuming an ideal system. The identification algorithm is initiated at $t = 0.42$ s and two stepwise changes occur: From $8.8 \mu\text{F}$ to $7 \mu\text{F}$ in the filter capacitance C_f at $t = 1.2$ s and from 6 mH to 3 mH in the grid-side inductance L_{gt} at $t = 2.4$ s.

V. RESULTS

The proposed identification method (cf. Fig. 5) is evaluated by means of simulations and experiments using a 50-Hz 12.5-kVA grid converter system. During the identification, the converter is controlled using a state-feedback current controller [5] tuned according to Appendix C. The switching frequency of the converter is 5 kHz and the sampling frequency is 10 kHz. A MLBS generated with 9 shift registers is used [20]. The amplitude of the MLBS is selected as ± 0.1 p.u. and it is generated at a frequency equal to the sampling frequency. The converter is operating under constant load of 0.8 p.u. The base value of voltage is $\sqrt{2/3} \cdot 400$ V and the base value of current is $\sqrt{2} \cdot 18$ A. The length of the mSDFT buffer is selected as $N = 200$ to match the lowest trackable harmonic frequency with the fundamental frequency of the grid voltage. The initial values of the mSDFT sample buffer are set to zero.

A. Simulation: Validating the Proposed Identification Method

A simulation model of the system shown in Fig. 4 was built for validating the presented method. Initially, no grid harmonics or losses of the filter components are included in the model. For validation, the PWM is modeled as a zero-order hold as assumed in the system model. Some noise is assumed in the identification model (7), and thus white noise with standard deviation of 0.002 p.u. is included in the current and voltage measurements. A simulation case with a constant forgetting factor of $\lambda = 0.995$ is presented in Fig. 7. The identification algorithm is initiated at $t = 0.42$ s. In the figure, a stepwise change of filter capacitance C_f from $8.8 \mu\text{F}$ to $7 \mu\text{F}$ occurs at $t = 1.2$ s and a similar stepwise change of grid-side inductance L_{gt} from 6 mH to 3 mH occurs at $t = 2.4$ s. The nominal values of the estimated parameters are given by the red dashed lines. While the parameters remain constant and the estimation is not in a transient state, the average relative errors of the estimates with respect to their nominal values are all 0%.

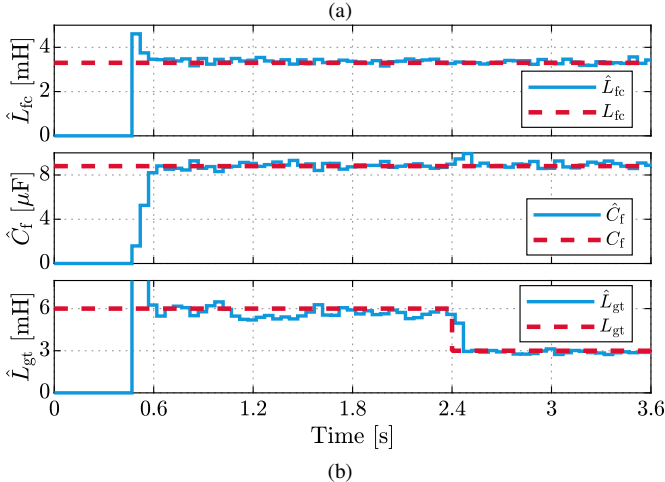
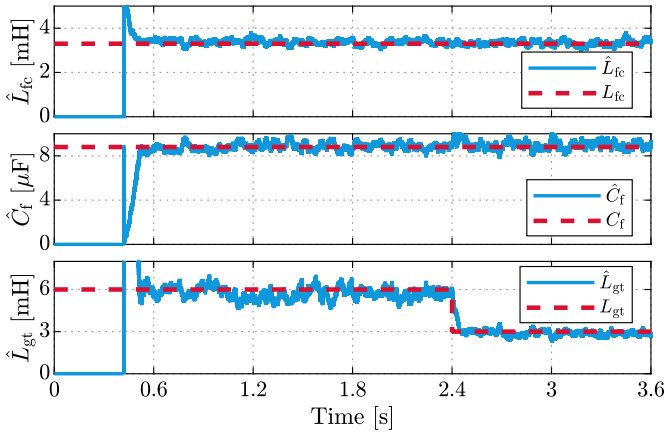


Fig. 8. Simulated evolution of the LCL filter parameter estimates with a) $\lambda = 0.995$ and b) variable forgetting factor. The identification algorithm is initiated at $t = 0.42$ s and a stepwise change from 6 mH to 3 mH occurs in the grid-side inductance L_{gt} at $t = 2.4$ s.

B. Simulation: Stepwise Change in the Grid-side Inductance

The simulation model was modified to include grid harmonics and inductor losses. The grid harmonics consist of 5th and 7th harmonics and both have an amplitude of 0.05 p.u. The filter inductors are modeled to include the effects of DC resistance and eddy currents. Therefore, they are modeled as an inductance parallel to a resistance and a resistance in series with the parallel connection of the resistance and the inductance [17]. For the converter-side inductor, the resistance value for the series resistor is $R_{c,s} = 102$ m Ω and for the parallel resistor $R_{c,p} = 420$ Ω . Similarly for the grid-side inductor, $R_{g,s} = 68$ m Ω and $R_{g,p} = 630$ Ω . Measurement noise with standard deviation of 0.02 p.u. is added to the current and voltage measurements.

Two simulation cases are presented. In the first case, a constant forgetting factor of $\lambda = 0.995$ is used and in the second case, a variable forgetting factor according to (19) with $x = 0.01$ is used to regularly modify the covariance matrix every $M = 500$ samples. The evolution of the parameter estimates for constant and variable forgetting factor are presented in Figs. 8a and 8b, respectively. In the figures, a stepwise

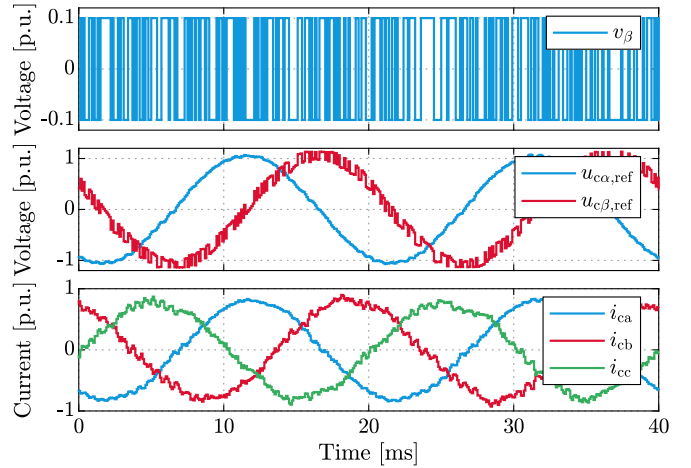


Fig. 9. Measured MLBS excitation signal (first), the space-vector components of the converter voltage reference (second), and the converter phase currents (third).

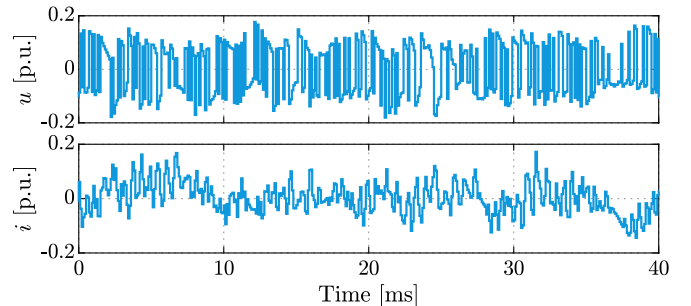


Fig. 10. Sequences of preprocessed voltage u (first) and current i (second) used in the RPE method.

change in the grid-side inductance L_{gt} from 6 mH to 3 mH occurs at $t = 2.4$ s. After the stepwise parameter change, the average relative errors of the parameter estimates with respect to their nominal values are 3% for \hat{L}_{fc} , 3% for \hat{C}_f , and 5% for \hat{L}_{gt} for constant forgetting factor. The corresponding values for variable forgetting factor are 2% for \hat{L}_{fc} , 2% for \hat{C}_f , and 5% for \hat{L}_{gt} . Out of the added non-idealities, the increased measurement noise induces the greatest error to the parameter estimates while the effect of grid harmonics is roughly 0%. The resistances cause relative errors of 1% on the inductance estimates.

C. Experiment: Stepwise Change in the Grid-side Inductance

The estimation cases presented in Figs. 8a and 8b are repeated experimentally. Fig. 9 shows the injected MLBS excitation v_β , the converter voltage reference components $u_{c\alpha,ref}$ and $u_{c\beta,ref}$, and the converter phase currents i_{ca} , i_{cb} , and i_{cc} , when the MLBS is active. Fig. 10 shows the preprocessed current and voltage sequences i and u from which the grid-frequency harmonics $m = [0, 1, 5, 7]$ have been removed. These current and voltage sequences are used as an input to the RPE algorithm.

The evolution of the parameter estimates for constant and variable forgetting factor are presented in Figs. 11a and 11b,

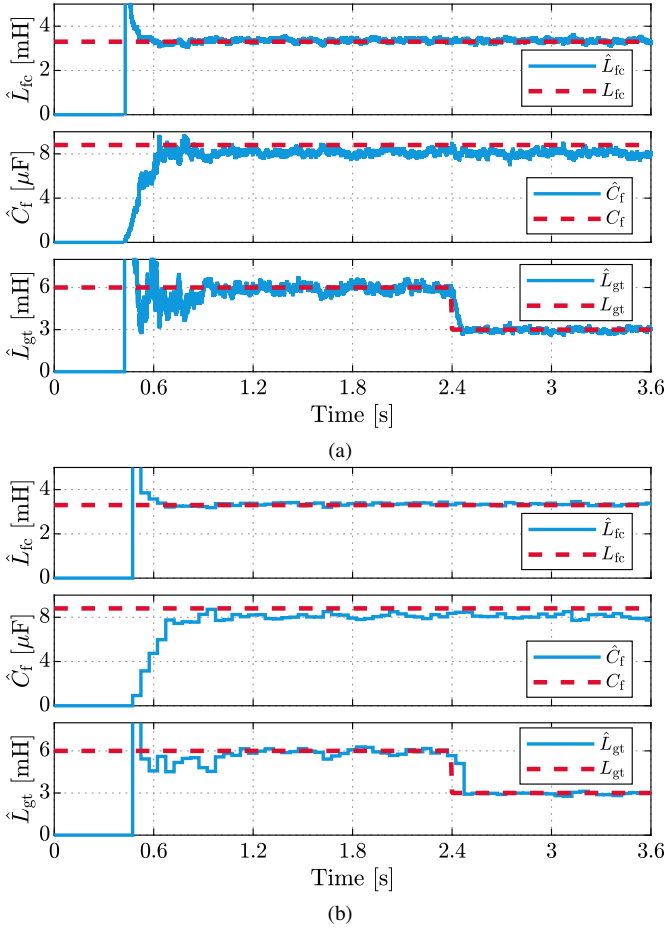


Fig. 11. Evolution of the LCL filter parameter estimates with a) $\lambda = 0.995$ and b) variable forgetting factor. The identification algorithm is initiated at $t = 0.42$ s and a stepwise change from 6 mH to 3 mH occurs in the grid-side inductance L_{gt} at $t = 2.4$ s.

respectively. After the stepwise change of the grid-side inductance, the average relative errors of the parameter estimates with respect to their nominal values are approximately equal in both cases, and they are 2% for \hat{L}_{fc} , 8% for \hat{C}_f , and 4% for \hat{L}_{gt} .

D. Discussion

Based on the simulation and experimental results, the method converges to correct estimates from its initial state and it is capable of tracking time-varying LCL filter parameters with good accuracy with either constant or variable forgetting factor. Overall, the variable forgetting factor used to modify the covariance matrix during operation yields slightly more consistent estimates with reduced computational effort due to updating the parameter estimates only once every M samples. The drawback of using variable forgetting factor over the constant forgetting factor, however, is that the parameter variations are not immediately seen in the estimates.

As the estimation result obtained from the ideal simulation model shows, the identification method yields exact estimates in an ideal case. Therefore, the estimation errors in the experiments are caused by unmodeled dynamics, nonlinearities

of the system, unbalances in the filter components, and inaccuracies in the transfer characteristics of the actuator and the measurement devices, as also seen in the simulations including some of these non-idealities.

Even though the estimates are found out to consistently converge to correct estimates, this result cannot be generalized for every system. Therefore, for systems where convergence issues arise, a slightly modified version of the RPE algorithm should be used for obtaining initial rough estimates. This modification is accomplished by setting the estimates of the noise polynomials zero, i.e., $\hat{c}_1 = 0$ and $\hat{c}_2 = 0$, in the equations for calculating the approximate gradient (28). After the transients in the estimates have settled, the approximate gradient should be calculated normally according to (28).

VI. CONCLUSIONS

This paper presents a real-time identification method for the inductances and the capacitance of LCL filters used in grid converters. Furthermore, the method indirectly estimates the grid inductance as a part of the grid-side inductance. The method can be embedded to a control system of PWM-based converters in a plug-in manner. An SDFT algorithm is used for computing the grid-frequency harmonics to enable computationally efficient real-time harmonic computation. A single recursive parameter estimation algorithm is used to estimate the identification model parameters. Two different methods are presented to enable tracking of time-varying parameters with the recursive parameter estimation algorithm by preventing the covariance wind-up phenomenon. Simulation and experimental results show that the parameters are estimated with good accuracy and parameter variations are detected.

APPENDIX A

DISCRETE-TIME MODEL OF THE LCL FILTER

A discrete-time model of an ideal LCL filter in stationary coordinates is presented below. The state vector is selected as $\mathbf{x} = [\mathbf{i}_c, \mathbf{u}_f, \mathbf{i}_g]^T$. The sampling of the converter currents and grid voltages is synchronized with the PWM, which is modeled as a zero-order hold. Under these assumptions, the system matrix Φ and the input vector Γ_c required for solving $Y_c(z)$ are

$$\Phi = \begin{bmatrix} \frac{L_{fc} + L_{gt} \cos(\omega_p T_s)}{L_{fc} + L_{gt}} & -\frac{\sin(\omega_p T_s)}{\omega_p L_{fc}} & \frac{L_{gt}[1 - \cos(\omega_p T_s)]}{L_{fc} + L_{gt}} \\ \frac{\sin(\omega_p T_s)}{\omega_p C_f} & \cos(\omega_p T_s) & -\frac{\sin(\omega_p T_s)}{\omega_p C_f} \\ \frac{L_{fc}[1 - \cos(\omega_p T_s)]}{L_{fc} + L_{gt}} & \frac{\sin(\omega_p T_s)}{\omega_p L_{gt}} & \frac{L_{gt} + L_{fc} \cos(\omega_p T_s)}{L_{fc} + L_{gt}} \end{bmatrix} \quad (21)$$

and

$$\Gamma_c = \frac{1}{L_{fc} + L_{gt}} \begin{bmatrix} T_s + \frac{L_{gt} \sin(\omega_p T_s)}{\omega_p L_{fc}} \\ L_{gt}[1 - \cos(\omega_p T_s)] \\ T_s - \frac{\sin(\omega_p T_s)}{\omega_p} \end{bmatrix} \quad (22)$$

The closed-form expression for the input matrix Γ_g can be found in [5].

APPENDIX B
RECURSIVE PREDICTION ERROR METHOD

The RPE algorithm [24] is presented below. It calculates an estimate $\hat{\theta} = [\hat{a}_1, \hat{b}_1, \hat{b}_2, \hat{c}_1, \hat{c}_2]^T$ based on the prediction error

$$\hat{e}(k) = y(k) - \hat{\varphi}^T(k)\hat{\theta}(k-1) \quad (23)$$

where $\hat{\varphi}(k)$ is the regressor vector (11) with true noise terms $e(k-1)$ and $e(k-2)$ replaced with their estimated values $\hat{e}(k-1)$ and $\hat{e}(k-2)$, respectively. The parameter vector is estimated recursively as

$$\hat{\theta}(k) = \hat{\theta}(k-1) + \mathbf{K}(k)\hat{e}(k) \quad (24)$$

where the gain \mathbf{K} is calculated as

$$\mathbf{K}(k) = \mathbf{P}(k)\psi(k) = \frac{\mathbf{P}(k-1)\psi(k)}{\lambda + \psi^T(k)\mathbf{P}(k-1)\psi(k)} \quad (25)$$

$$\mathbf{P}(k) = \frac{\mathbf{P}(k-1)}{\lambda} - \frac{\mathbf{P}(k-1)\psi(k)\psi^T(k)\mathbf{P}(k-1)}{\lambda[\lambda + \psi^T(k)\mathbf{P}(k-1)\psi(k)]} \quad (26)$$

where $\psi(k)$ is an approximate gradient given by

$$\psi(k) = \begin{bmatrix} i_F(k-2) - i_F(k-1) \\ u_F(k-2) + u_F(k-4) \\ u_F(k-3) \\ \hat{e}_F(k-1) \\ \hat{e}_F(k-2) \end{bmatrix} \quad (27)$$

where

$$\begin{aligned} i_F(k) &= i(k) - \hat{c}_1(k)i_F(k-1) - \hat{c}_2(k)i_F(k-2) \\ u_F(k) &= u(k) - \hat{c}_1(k)u_F(k-1) - \hat{c}_2(k)u_F(k-2) \\ \hat{e}_F(k) &= \hat{e}(k) - \hat{c}_1(k)\hat{e}_F(k-1) - \hat{c}_2(k)\hat{e}_F(k-2) \end{aligned} \quad (28)$$

Initial values for $\hat{\theta}$ and \mathbf{P} are required in order to start the algorithm. The initial values are $\hat{\theta}(0) = 0$ and $\mathbf{P}(0) = \mathbf{I}$ p.u.

APPENDIX C

DESIGN PARAMETERS FOR THE CONTROL METHOD

The parameters for the observer-based current control method of [5] are $\omega_{cd} = 2\pi \cdot 150 \frac{\text{rad}}{\text{s}}$, $\zeta_{cd} = 1$, $\omega_{cr} = \omega_p$, $\zeta_{cr} = 0.01$, $\omega_{od} = 5\omega_{cd}$, $\zeta_{od} = 1$, $\omega_{or} = \omega_p - \omega_g$, and $\zeta_{or} = 0.7$. The notation follows that used in [5]. The synchronous reference frame of the control system was established using a SRF-PLL tuned with $\zeta_{PLL} = 0.7$ and $\omega_{PLL} = 2\pi \cdot 15 \frac{\text{rad}}{\text{s}}$. The DC-bus voltage is assumed constant.

For direct identification in closed-loop systems, the noise e affects the input signal u [cf. (7)] through the feedback loop and results in biased estimates [19]. The level of bias depends on the accuracy of the selected noise model and on the controller tuning. Therefore, reduced bandwidth and damping factors are used for the duration of the identification to reduce the bias caused by the feedback loop.

REFERENCES

- [1] M. Liserre, F. Blaabjerg, and S. Hansen, "Design and control of an LCL-filter-based three-phase active rectifier," *IEEE Trans. Ind. Appl.*, vol. 41, no. 5, pp. 1281–1291, 2005.
- [2] V. Blasko and V. Kaura, "A novel control to actively damp resonance in input LC filter of a three-phase voltage source converter," *IEEE Trans. Ind. Appl.*, vol. 33, no. 2, pp. 542–550, 1997.

- [3] C. A. Busada, S. G. Jorge, and J. A. Solsona, "Full-state feedback equivalent controller for active damping in LCL-filtered grid-connected inverters using a reduced number of sensors," *IEEE Trans. Ind. Electron.*, vol. 62, no. 10, pp. 5993–6002, 2015.
- [4] J. Dannehl, F. W. Fuchs, S. Hansen, and P. B. Thogersen, "Investigation of active damping approaches for PI-based current control of grid-connected pulse width modulation converters with LCL filters," *IEEE Trans. Ind. Appl.*, vol. 46, no. 4, pp. 1509–1517, 2010.
- [5] J. Kukkola, M. Hinkkanen, and K. Zenger, "Observer-based state-space current controller for a grid converter equipped with an LCL filter: Analytical method for direct discrete-time design," *IEEE Trans. Ind. Appl.*, vol. 51, no. 5, pp. 4079–4090, 2015.
- [6] K. J. Åström and B. Wittenmark, *Adaptive Control*, 2nd ed. Boston, MA, USA: Addison-Wesley Longman Publishing Co., Inc., 1994.
- [7] H. Soliman, H. Wang, and F. Blaabjerg, "A review of the condition monitoring of capacitors in power electronic converters," *IEEE Trans. Ind. Appl.*, vol. 52, no. 6, pp. 4976–4989, 2016.
- [8] T. Roinila, M. Vilkkko, and J. Sun, "Online grid impedance measurement using discrete-interval binary sequence injection," *IEEE Trans. Emerg. Sel. Topics Power Electron.*, vol. 2, no. 4, pp. 985–993, 2014.
- [9] S. Cobreces, E. J. Bueno, D. Pizarro, F. J. Rodriguez, and F. Huerta, "Grid impedance monitoring system for distributed power generation electronic interfaces," *IEEE Trans. Instrum. Meas.*, vol. 58, no. 9, pp. 3112–3121, 2009.
- [10] P. Garcia, M. Sumner, Á. Navarro-Rodríguez, J. M. Guerrero, and J. Garcia, "Observer-based pulsed signal injection for grid impedance estimation in three-phase systems," *IEEE Trans. Ind. Electron.*, vol. 65, no. 10, pp. 7888–7899, 2018.
- [11] B. Arif, L. Tarisciotti, P. Zanchetta, J. C. Clare, and M. Degano, "Grid parameter estimation using model predictive direct power control," *IEEE Trans. Ind. Appl.*, vol. 51, no. 6, pp. 4614–4622, 2015.
- [12] N. Hoffmann and F. W. Fuchs, "Minimal invasive equivalent grid impedance estimation in inductive-resistive power networks using extended Kalman filter," *IEEE Trans. Power Electron.*, vol. 29, no. 2, pp. 631–641, 2014.
- [13] D. K. Alves, R. Ribeiro, F. B. Costa, and T. O. A. Rocha, "Real-time wavelet-based grid impedance estimation method," *IEEE Trans. Ind. Electron.*, 2018, early access.
- [14] F. Huerta, S. Cobreces, F. Rodríguez, D. Pizarro, and F. Meca, "Black-box identification for an auto-tuned current controller working with voltage source converters connected to the grid through a LCL filter," in *Proc. IEEE ISIE*, Bari, Italy, 2010, pp. 96–101.
- [15] F. Huerta, S. Cobreces, F. Rodriguez, M. Moranchel, and I. Sanz, "State-space black-box model identification of a voltage-source converter with LCL filter," in *Proc. IEEE PEDG*, Aalborg, Denmark, 2012, pp. 550–557.
- [16] F. Huerta, S. Cobreces, F. Rodríguez, C. Clancey, and I. Sanz, "Comparison of two black-box model identification methods applied on a VSC with LCL filter," in *Proc. IEEE IECON*, Montreal, Canada, 2012, pp. 4648–4653.
- [17] J. Koppinen, J. Kukkola, and M. Hinkkanen, "Parameter estimation of an LCL filter for control of grid converters," in *Proc. IEEE ICPE-ECCE*, Seoul, South Korea, 2015, pp. 1260–1267.
- [18] —, "Plug-in identification method for an LCL filter of a grid converter," *IEEE Trans. Ind. Electron.*, vol. 65, no. 8, pp. 6270–6280, 2018.
- [19] L. Ljung, *System Identification: Theory for the User*, 2nd ed. Troy, NY, USA: Prentice-Hall, 1999.
- [20] T. Roinila, M. Vilkkko, and J. Sun, "Broadband methods for online grid impedance measurement," in *IEEE ECCE*, 2013, pp. 3003–3010.
- [21] J. G. Proakis and D. K. Manolakis, *Digital Signal Processing*, 4th ed. Upper Saddle River, NJ, USA: Prentice-Hall, Inc., 2006.
- [22] E. Jacobsen and R. Lyons, "The sliding DFT," *IEEE Signal. Proc. Mag.*, vol. 20, no. 2, pp. 74–80, 2003.
- [23] K. Duda, "Accurate, guaranteed stable, sliding discrete Fourier transform [DSP tips & tricks]," *IEEE Signal. Proc. Mag.*, vol. 27, no. 6, pp. 124–127, 2010.
- [24] T. Söderström and P. Stoica, *System Identification*. London, UK: Prentice-Hall, 1989.
- [25] M. Tham and S. Mansoori, "Covariance resetting in recursive least squares estimation," in *Proc. IET Int. Conf. Control*, Oxford, UK, 1988, pp. 128–133.